Light-Diffraction Particle Size Measurements in Small Solid-Propellant Rockets

E. D. Youngborg,* T. E. Pruitt,* M. J. Smith,† and D. W. Netzer‡
Naval Postgraduate School, Monterey, California

An experimental investigation was conducted to determine the effects of operating pressure and position within the motor and exhaust nozzle on the particle size distribution for a reduced smoke propellant. Light-diffraction measurements were made in a small solid-propellant rocket motor and high-speed motion pictures of strand burners were taken. Particle sizes were measured near the propellant surface of the end-burning grain, at the nozzle entrance, and at the nozzle exit. The results indicated that much of the ZrC reacts on or very near to the propellant surface to form ZrO_2. Small particles (probably ZrC) were ejected from the propellant surface without agglomeration and were consumed, whereas the large agglomerates (probably ZrO_2) remained almost constant in size along the length of the motor. The particulates broke up in the nozzle converging section to a monomodal distribution with a D_{32} between 15 and 19 μm, independent of the particle size entering the nozzle. Aft of the nozzle in the expanding plume, the particles were significantly smaller and had multimodal distributions. It was also found that assuming a monomodal distribution of particles, when the distribution is actually multimodal, can lead to significant errors in measuring D_{32} from scattered light-intensity profiles.

Introduction

USE of reduced/minimum smoke propellants in tactical applications often requires small amounts of additives, such as zirconium, zirconium carbide, or aluminum oxide, to provide acoustic stabilization. The acoustic damping provided is highly dependent on particle size. These additives also introduce certain loss mechanisms.[1] The delivered impulse is generally reduced by incomplete metal combustion and two-phase flow losses in the exhaust nozzle. Exhaust plume signature can also be dependent upon the particle size distribution; especially if larger particles remain within the core region of the plume and are surrounded by smaller particles which can more readily track the gas flow. The larger particles can be expected to be at higher temperatures than the surrounding gas, with the associated increase in radiation. To accurately predict these performance effects requires accurate knowledge of the particle sizes throughout the motor and exhaust nozzle.

Several computer codes attempt to model the combustion process in order to predict solid rocket motor performance. The SPP (solid performance program)[2] is one such code. These programs are semiempirical in nature and require an a priori knowledge of the particle size distribution entering the exhaust nozzle. This distribution must be experimentally determined[3] because this information cannot be predicted by current analytic methods.

A specific problem in predicting the exhaust signature is the accurate prediction of particle breakup, condensation, and/or agglomeration within the exhaust nozzle and plume. Analytical models for these processes have not been validated with direct measurements. Data are needed on the effects of the metal powder size and composition cast into the propellant, the particle size distribution entering the nozzle, the nozzle geometry and the nozzle area ratio on the particulate processes, and the exhaust particle size distribution. Essentially no data are available except for limited measurements which have been made in exhaust plumes.

Collecting exhaust products from strand burners and motors, light-transmission measurements, light-scattering measurements, holography, high-speed motion pictures, and schlieren and laser schlierens have all been used to study solid propellant combustion at the Naval Postgraduate School.[1] The present investigation focused on the use of light-scattering techniques to determine particle size. The light-scattering measurement method is nonintrusive and suited to measurements in both the motor and exhaust nozzle environments. Some high-speed motion pictures were also used to validate conclusions reached about surface behavior. The speed of the flow precludes successful application of most holographic techniques within the exhaust nozzle.

Zirconium carbide is often used as a stability additive. However, it is not known whether surface agglomeration occurs, or whether the zirconium burns to zirconium oxide. Both of these processes affect the size distribution and density of the particles in the gas phase, which in turn affect the ability to provide damping for a specific frequency of pressure oscillation. The goal of this investigation was to determine the effects of operating pressure and position within the motor and exhaust nozzle on the particle size distributions from a reduced smoke propellant.

Theoretical Background

The particle sizing method chosen for the present research was based upon ensemble-averaged, near-forward light diffraction. Near-forward light-scattering measurements have the advantage of being practically independent of the particle index of refraction. Ensemble-averaged measurements permit particle sizing in flows with high particle concentrations, independent of particle velocity or position. Size distributions can also be measured, but with somewhat more detailed data analysis.[4,5] Some limitations of the technique are that no spatial distribution and/or velocity data are obtained, and viewing windows must be kept very clean.

The scattering and absorption of a plane monochromatic electromagnetic wave by an isotropic homogeneous sphere is described by Mie's solution to Maxwell's equations,[6] and the general theory of scattering developed by Mie is presented by Van de Hulst.[7] The characteristics of scattered light depend upon the particle size, shape, internal structure, refractive

Received Oct. 31, 1988; revision received March 2, 1989.

*Graduate Student, Lieutenant Commander, U.S. Navy.
†Graduate Student, Captain, U.S. Army.
‡Professor, Department of Aeronautics and Astronautics. Member AIAA.

index with respect to the surrounding medium, the scattering angle, and the incident wave polarization and wavelength.[6-8]

When the particle diameters differ significantly from the wavelength of the incident light, the solutions simplify to Fraunhofer diffraction (for large particles) and Rayleigh scattering (for smaller particles). Fraunhofer diffraction is applicable to the larger particles because diffraction dominates the forward scattered light in the center lobe. It has been shown that diffraction measurements can be successfully used for particles as small as 1 μm.[9-11] This is generally accomplished using intensity or energy-ratioing techniques. Thus, measurements of diffracted light can be used for measuring the particles which are of significance for particle damping and two-phase flow losses and, also, for many of the particles which are important in determination of exhaust plume signature.

The classical result of Fraunhofer diffraction from a single particle, i.e., the discrete Airy diffraction pattern, is not typically observed in practical combustion experiments when ensemble-sizing techniques are used because the particulates are polydispersed and, in many cases, a multimodal distribution is present. The intensity distribution of diffractively scattered light from a particle is given by[6-8]

$$I(\theta)/I_0 = (\alpha^2 D^2/16)[2J_1(\alpha \sin\theta)/\alpha \sin\theta]^2 \tag{1}$$

where J_1 is the first-order Bessel function, $\alpha = \pi D/\lambda$, θ is the scattering angle from the forward direction, D is the particle diameter, λ is the wavelength of the incident light, $I(\theta)$ is the intensity of scattered light at angle θ, and I_0 is the intensity of the incident illumination. Considering only small angles ($\theta \lesssim 15$ deg), and normalizing by the forward-scattered light at $\theta = 0$,

$$I(\theta)/I(0) = [2J_1(\alpha\theta)/\alpha\theta]^2 \tag{2}$$

The normalized integrated intensity of forward scattered light from a polydispersion of large particles is given as[12]

$$\frac{I(\theta)}{I(0)} = \frac{\int_0^{D_\infty} \left[\frac{2J_1(\alpha\theta)}{(\alpha\theta)}\right]^2 N_r(D) D^4 \, dD}{\int_0^{D_\infty} N_r(D) D^4 \, dD} \tag{3}$$

where $N_r(D)$ is a distribution function describing the proportion of particles with diameter D in the sample. The upper limit distribution function (ULDF) developed by Mugele and Evans[13] was used by Dobbins et al.,[12] and the same approach was followed in a portion of this investigation. The volume-to-surface mean diameter (Sauter mean diameter) D_{32} of a polydispersion is defined by

$$D_{32} = \frac{\int_0^{D_\infty} N_r(D) D^3 \, dD}{\int_0^{D_\infty} N_r(D) D^2 \, dD} \tag{4}$$

Scattering intensity profiles for different size distributions of the ULDF plotted against ($\pi D_{32}\theta/\lambda$) are brought into near coincidence.[12] Buchele[14] showed that for $\pi D_{32}\theta/\lambda < 3$, a Gaussian profile closely matches the theoretical intensity profile for a polydispersion obtained by integrating Eq. (3). The Gaussian expression presented by Buchele is given as

$$\frac{I(\theta)}{I(0)} = \exp[-(0.57\ \pi D_{32}\theta/\lambda)^2] \tag{5}$$

The data-reduction technique developed by Harris[15] and Netzer and Powers[1] was based on Buchele's work. This method involves comparison of the experimentally obtained intensity profile with Eq. (5) which requires the value of $I(0)$. Since transmitted light dominates at very low scattering angles, $I(0)$ cannot be measured. A ratioing technique eliminates this problem. Equation (5) can be used to ratio $I(\theta_2)/I(\theta_1)$ as follows

$$\frac{I(\theta_2)}{I(\theta_1)} = \exp\left[-D_{32}^2\left(\frac{0.57\pi}{\lambda}\right)^2(\theta_2^2 - \theta_1^2)\right] \tag{6}$$

However, $I(\theta_1)$ at the "minimum" forward angle θ_1 must be taken from the experimentally measured profile at a location where significant transmitted light effects are not present. The resultant profile $I(\theta_2)/I(\theta_1)$ vs θ_2 can then be generated for a specified D_{32}. D_{32} is determined by the trial and error matching of Eq. (6) to the measured profile. However, this approach has an obvious disadvantage of being limited to monomodal distributions.

Experimental Apparatus

The series of experiments were conducted using two small-windowed solid-propellant rocket motors with end-burning grains. The chamber diameter was 2.00 in. and the propellant was 1.00-1.25-in. thick. A long motor was used to obtain measurements of particle size prior to the nozzle entrance and in the exhaust. A short motor was used to obtain particle size measurements just above the propellant burning surface. Additional details of the motor designs are found in Ref. 18. The windows were flushed by a nitrogen purge that was distributed uniformly in the window ports using a sintered metal sleeve. The investigation used a reduced smoke propellant provided by the Naval Weapons Center, China Lake, California (Table 1).

Two laser-diffraction systems were utilized. One system was locally designed (called the NPS system) and the other was a Malvern 2600 HSD particle sizer. Two systems were utilized in order to obtain particle size data at two locations during one test. The Malvern system was preferred, but two units could not be used simultaneously with the small motors. The NPS system required very little space, and was very inexpensive to construct and maintain. Several limitations of the NPS system are discussed below.

The NPS system used an 8-mW He-Ne laser source. The scattered light passed through a wide-pass laser line filter and a 500-mm focal length Fourier transform lens, which focused the light onto a linear photodiode array (Reticon RL 1024G) having 1024 photodiodes on 25-μm centers. The array was scanned at a rate of 33 kHz and a 6-ms blanking pulse was used to sequence the sweeps. The range of scattering angles within the field of view is determined by a number of factors. The maximum scattering angle is determined by the diameter and focal length of the focusing lens, the distance between the focusing lens and the particles, the diameter of the motor window, and the height/position of the diode array.[1] The minimum scattering angle is determined when significant amounts of unscattered light are superimposed on the scattered light (approximately 0.01 rad in the present apparatus). The range of scattering angles for this investigation was either 0.01-0.06 rad or 0.02-0.07 rad. A limitation of the NPS system was the very small detector areas. This resulted in signal-to-noise ratios which prevented the system from measuring very weak scattering intensities. A complete description of the apparatus is contained in Refs. 1 and 18.

Prior to a motor firing, a background measurement was recorded. This background intensity profile was then subtracted from the intensity profile measured with particles pre-

Table 1 Major propellant ingredients

Ingredients	Approximate wt. %
R45M	8.9
RDX	4.0
AP (11 μm)	25.0
AP (200 μm)	57.0
ZrC (2-20 μm, $D_{32} = 5.1$ μm)	1.0

sent. This procedure accounted for noise from ambient light and corrected for the characteristics of individual diodes. Raw data were displayed on a CRT so that any erroneous scans could be excluded prior to data reduction.

A symmetric moving-average-type digital filter was then applied to the NPS profile in order to smooth the curve.[15] The chief disadvantage of the method lies in the fact that there is no way to account for the actual distribution of the particulates. The Sauter mean diameter (SMD) determined by this algorithm is associated with the dominant mode (within the field of view of the array) of a multimodal polydispersed sample.

The Malvern particle sizer is similarly based upon Fraunhofer diffraction.[4] However, it uses the measured scattering profile to obtain a particle size distribution. The Malvern approach allows selecting the type of particle size distribution (Rosin-Rammler, log-normal, normal) or a model-independent mode. The latter provides the ability to measure multimodal particle size distributions. The Malvern technique[4,17] is based upon a discretized form of an equation similar to the numerator of Eq. (3) in which the scattered light from 32 discrete particle sizes is measured at 31 separate scattering angles. Inversion techniques and a constrained least-squares fitting technique are used to obtain the best fit between the measured and theoretical profiles. Dodge et al.[16] showed good agreement between data obtained using the Malvern and several single-particle counters. The Malvern utilizes a 2-mW He-Ne laser with a collimated beam diameter of 9 mm. One of the principle advantages of the Malvern system is its use of an annular photodiode array consisting of 31 rings. Ring arrays permit much weaker intensities to be measured than can be accomplished with linear arrays. A 100-mm focal length Fourier transform lens was used for the current set of experiments, with a particle range from 1.9–188 μm.

The high-speed motion pictures utilized a Hycam camera with framing rates between 6000 and 10,000 pps. Small strands (7–10 mm wide × 1–3 mm thick × 10 mm high) were burned in a nitrogen purged, windowed combustion bomb. Side lighting was provided with a 1200-W tungsten filament lamp.

Results and Discussion

The Sauter mean diameter (D_{32}) was the common measured parameter between the NPS and Malvern systems. The distinct advantage of being able to characterize multimodal particle size distributions made the Malvern the better suited instrument for the through-motor measurements. In the exhaust, the annular detector of the Malvern system allowed for the measurement of much weaker intensities as opposed to the NPS system.

System Calibration

Among the methods available for calibration of laser-diffraction instruments, the more commonly used include the calibration reticle and commericially prepared samples of known diameters. The latter approach was used in this investigation because a wider range of particle sizes and distributions could be utilized. The types of samples used included polystyrene spheres, glass beads, and aluminum oxide powders. In each case, the sample material was suspended in a solution of distilled water.

The NPS system was calibrated using distributions of polystyrene spheres, with diameters centered at 5.1, 9.6, or 20.0 μm. The Malvern 2600 was calibrated using polystyrene spheres, glass beads, and an aluminum oxide powder. The results presented in Table 2 demonstrate good agreement for both systems.

To examine the ability of the Malvern to correctly characterize a multimodal distribution, a polydispersed bimodal sample centered at 5.1 and 20.0 μm was prepared. The measured distribution of the sample shown in Fig. 1 indicates that the bimodal distribution was correctly determined.

When multiple scattering becomes significant, the mean particle diameters determined from single-scattering theory are too small. Gulder[19] has determined empirical corrections for D_{32} for Malvern data when obscurations are greater than 0.5. These corrections were utilized for D_{32}, when required, for the through-motor measurements in the present investigation. It should also be noted that if large amounts of submicron particles are present together with the larger particles, both systems will yield data only for the larger particles.

Table 2 Calibration results

Particle material	Median diameter, μm	Range of diameters, μm ($\pm 2\sigma$)	Scattering measurement D_{32}, μm	
			NPS	Malvern
Polystyrene	5.1[a]	4.6–6.4[a]	5.4	5.5
Polystyrene	9.6[a]	8.5–10.4[a]	9.4	—
Polystyrene	20.0[a]	14.9–24.4[a]	20–21	20.8
Aluminum oxide	5–8[b]	1–20[b]	—	7.3
Glass beads	40[b]	37–44[b]	—	40.1

[a]Manufacturer's data (Duke Scientific Corporation). [b]Manufacturer's data.

Behavior of ZrC

The experiments covered a range of pressures from approximately 70–450 psig and were centered into classes of 150, 250, and 400 psig. For each class, scattering measurements were made 1) near the grain (end burning), 2) prior to the nozzle

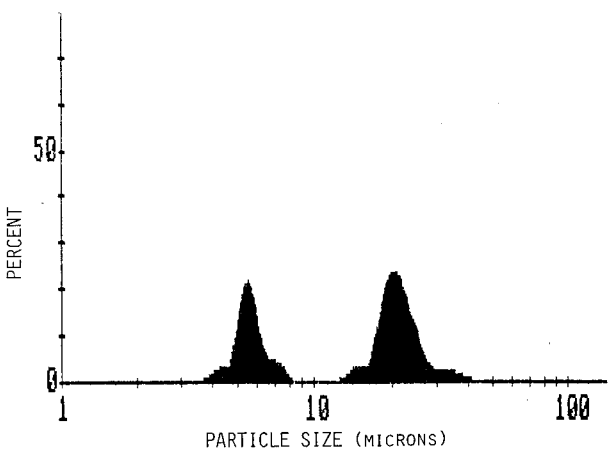

Fig. 1 Calibration using 5.1- and 20.0-μm particles; volume distribution.

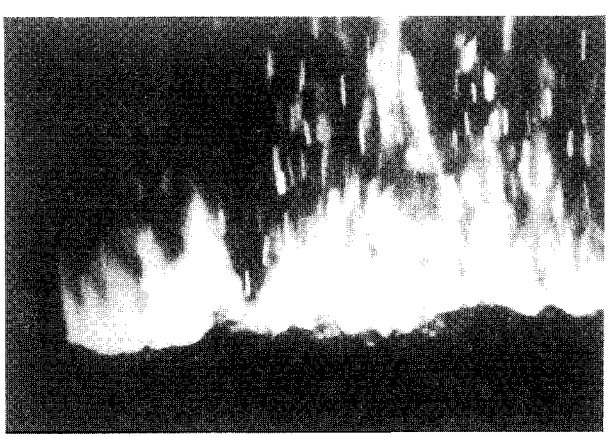

Fig. 2 Photograph of 1% ZrC propellant strand burning at 500 psi (strand width = 7 mm).

entrance, 3) at the exhaust with $P_e = P_{critical}$, and 4) at the exhaust with $P_e = P_o$.

Zirconium carbide has been observed to burn vigorously on the surface of reduced smoke propellants containing ammonium perchlorate (AP) and hydroxy-terminated polybutadiene (HTPB).[20] This behavior is also evident in Fig. 2 which shows a propellant strand burning at 500 psig. Large surface agglomerates are evident. Table 3 presents some of the relevant temperatures for zirconium compounds in the motor environment.

If zirconium carbide (ZrC) burns stoichiometrically with oxygen, the resulting temperature is much greater than the melting temperature of ZrO_2. If the carbon is stripped to form CO_2 (leaving a local surface of Zr or ZrO_2) then the Zr will probably burn in a surface reaction process, since the boiling temperature of Zr is very high and there is a high solubility of ZrO_2 in molten Zr.[21] The plausible combustion sequence for ZrC starts as the material is exposed at the burning surface. Here oxygen (O_2) from the ammonium perchlorate (AP) flame attacks the carbon to produce either carbon monoxide (CO) or carbon dioxide (CO_2), leaving exposed zirconium. Oxygen from water vapor may also be involved. The oxygen then reacts with the zirconium to produce a porous ZrO_2 surface layer.[21] The oxide should be a liquid since the local temperature at the particle surface (as a result of the surface combustion of ZrC or Zr with O_2) should be much greater than the melting temperature of ZrO_2. The adiabatic flame temperature was also close to the melting temperature of ZrO_2. The low burning rates associated with the relatively low chamber pressures used in this investigation apparently allowed sufficient time for the molten ZrO_2 on adjacent particles to agglomerate on the burning surface, prior to leaving the propellant surface. At higher burning rates (pressures), the particles would be ejected from the surface more rapidly and should result in smaller agglomerates.

Near-Propellant Surface Data

The test results obtained near the grain surface are summarized in Table 4. Note that all of the distributions were trimodal or quadmodal and that D_{32} (corrected for mutiple scattering effects) decreased significantly with increasing chamber pressure. The peaks of the distributions also showed that, as pressure increased, the larger agglomerates disappeared and the smaller particles increased in quantity. The existence of particulates in the (uncorrected) range of 3–4 μm indicates that some of the particulates were ejected directly into the gas stream without surface agglomeration. Figure 3 shows the typical trimodal distribution of particulates.

The initial high-speed motion pictures of strand burners were taken without filters or intense illumination to observe the burning behavior. Approximately 350 particles were "flame sized" from each film taken at 100 or 500 psi. The results are shown in Fig. 4. The flame diameters were approximately five times larger than the particulates. The film resolution was approximately 20 μm and the environments are somewhat different for strands and end-burning grains. However, the data in Fig. 4 show a shift to smaller diameters as pressure is increased, in agreement with the data in Table 4.

Nozzle Entrance Data

Table 5 presents the results from the measurements obtained prior to the nozzle entrance. At low pressures the distributions remained bimodal with the dominant modes centered at approximately 30 and 70 μm. Comparing the Sauter mean diameters (Fig. 5) and volume-distribution profiles for the near-grain and nozzle entrance measurements for approximately 150 psig revealed only small differences. The data in Tables 4 and 5 indicate that the small volume of small particles (which does not affect D_{32}) near the propellant surface were consumed along the length of the motor, whereas the larger particles remained practically constant in diameter. At slightly higher pressures (250 psig), the increased volume of small particles reduces D_{32} near the propellant surface. Their consumption together with the approximately constant-diameter larger particles resulted in an increase in D_{32} across the length of the motor. For pressures near 400 psi, the small particles were again consumed, leaving a monomodal distribution with a D_{32} of 14 μm at the nozzle entrance. This behavior along the length of the motor is consistent with the idea that the larger

Table 3 Thermophysical properties of Zr, ZrC, and ZrO_2

Material	Melting temperature, K	Boiling Temperature, K
Zr	2127 (Ref. 21)	4700 (Ref. 21)
ZrC	3523 (Ref. 22)	—
ZrO_2	2988 (Ref. 21)	4573 (Ref. 23)

Note: Adiabatic flame temperature for the propellant was determined to be 2916 K and the adiabatic flame temperature for the reaction $ZrC + 2O_2 \rightarrow ZrO_2 + CO_2$ is approximately 4400 K.

Table 4 Near grain-surface particle sizes (Malvern)

Pressure, psig	Throat diameter, in.	Corrected D_{32}, μm	Type of distribution	Peaks (uncorrected) of dominant modes, μm
159	0.200	64	Quadmodal/ Trimodal	3.5,[a] 12, 35, 65
188	0.200	73	Trimodal	3.5,[a] 27, 78
248	0.177	32	Trimodal	3.5, 12, 25
448	0.150	15	Trimodal	3.5,[b] 12, 25

[a]Small percentage of particle volume. [b]Large percentage of particle volume.

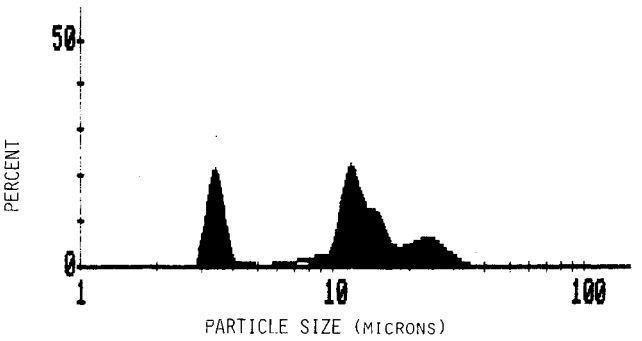

Fig. 3 Volume distribution near surface; P_c = 448 psig.

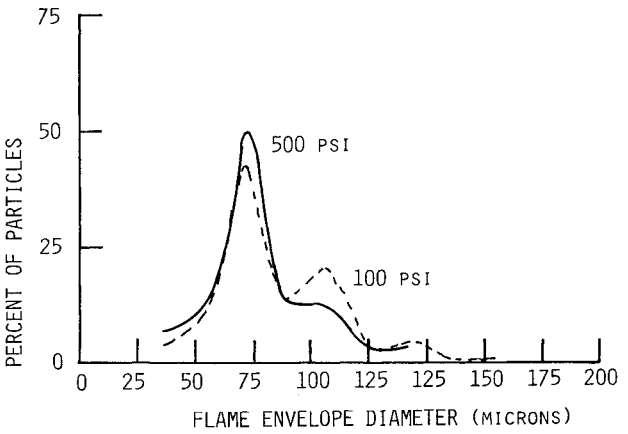

Fig. 4 Flame envelope diameter distributions from strands of 1% ZrC propellant.

Table 5 Motor chamber scattering measurements obtained upstream from nozzle converging section

Pressure, psig	t_{res}, ms	Corrected D_{32}, μm	Type of distribution	Peaks (uncorrected) of dominant modes, μm
79	47	38[a]	—	—
119	43	88	Bimodal	32, 70
124	49	81	Bimodal	27, 68
125	49	29[a]	—	—
135	49	30[a]	—	—
175	74	24[a]	—	—
251	79	48	Bimodal	15, 38
252	74	49	Bimodal	13, 47
300	93	19[a]	—	—
352	104	18[a]	—	—
370	86	32	Broad monomodal	19
427	117	28	Monomodal	14

[a]NPS laser-diffraction system data. All other data from Malvern.

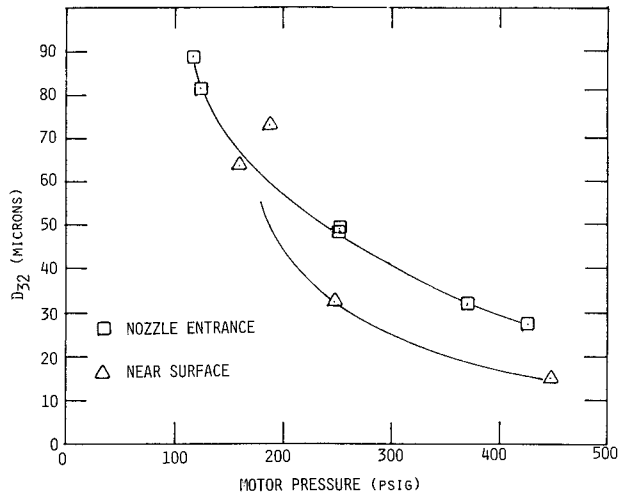

Fig. 5 D_{32} dependence on pressure (Malvern data).

agglomerates are ZrO_2 (or have a ZrO_2 surface layer), whereas the smaller particles are ZrC which is ejected directly from the propellant surface without agglomeration.

Exhaust Nozzle Data

Beam steering was often evident in the exhaust measurements. The procedure employed when using the Malvern master sizer program was to inhibit data from the affected inner rings. Care must be exercised in this procedure to ensure that no scattering data will be lost as a result of inhibiting data from the affected inner rings.

Table 6 presents results obtained in the exhaust for when the nozzle exit plane pressure equals the critical pressure (choked, converging nozzle). The nozzles used in these tests had a 45 deg converging section, a short (0.01-0.015 in.) tubular throat section, and no expansion cone. Figure 6 presents the results obtained at 370 psig using the NPS system. The distance downstream of the nozzle exit plane varied slightly as noted in Table 6, due to the geometry of the apparatus. All of the distributions were monomodal (Fig. 7) with the exception of the test at the lowest pressure (147 psig). Here, a second broadly distributed mode was observed which covered a range of approximately 4.5-12.0 μm. Except for this point, D_{32} varied only slightly as chamber pressure or residence time was increased (Fig. 8). Thus, the particles at the throat had a narrow band monomodal distribution which was independent of the upstream pressure and entering particulate sizes. This behavior indicates a critical Weber number is exceeded with sufficient time for the breakups to occur.[24]

Table 6 Exhaust scattering Measurements ($P_e = P_{critical}$)

Pressure, psig	Location behind nozzle exit, in.	D_{32}, μm	Type of distribution	Peaks of dominant modes, μm
147	1.1	8	Bimodal	10, 19
212	0.6	19	Narrow monomodal	19
370	2.7	16[a]	—	—
371	0.6	19	Narrow monomodal	19
421	0.6	19	Narrow monomodal	19
450	1.1	15	Narrow monomodal	15

[a]NPS laser-diffraction data. All other data from Malvern.

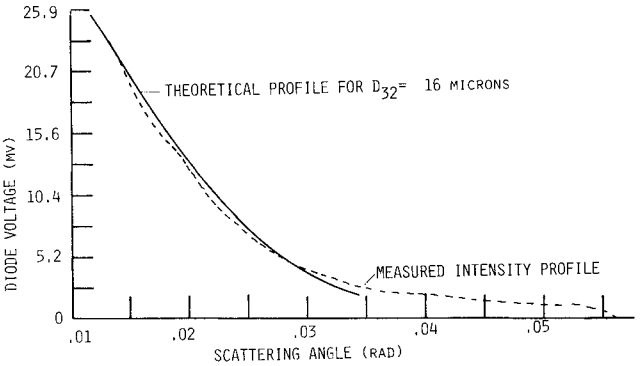

Fig. 6 Nozzle exhaust intensity profile using NPS apparatus; $P_e = P_{critical}$, 370 psig.

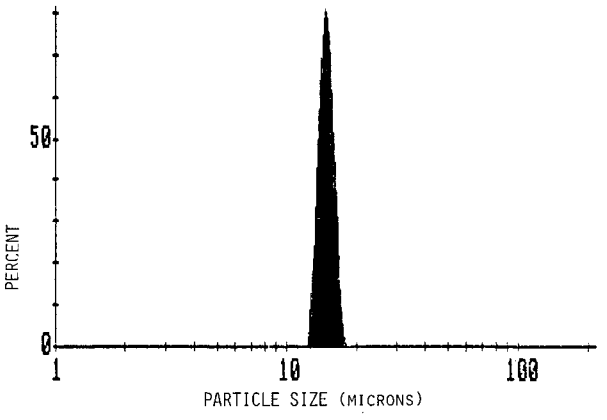

Fig. 7 Volume distribution in exhaust; $P_e = P_{critical}$, 450 psig.

The NPS data point in Fig. 8 was obtained simultaneously with upstream data. The agreement of D_{32} with and without window purge indicated that the low flow rate used for the purge (3-9% of gas flow in the motor) did not significantly affect the particulates across the 2-in. diameter of the motor. Table 7 contains the results obtained in the exhaust for the condition of nozzle exit pressure equal to ambient pressure. The nozzle exit Mach number was approximately 2 at a pressure of 100 psi and 4 at a pressure of 400 psi. Except for one test, the nozzles all had converging half-angles of 45 deg and diverging half-angles of 15 deg. All of the distributions were multimodal except for the test at 215 psig. In this test, the measurements were made 0.6 in. downstream of the nozzle exit plane vs 2.7 in. for all other tests. The 2.7-in. distance was determined by apparatus constraints when data were being obtained simultaneously through the motor. The data point obtained 0.6 in. downstream may indicate that the majority of the particles remained monomodal and essentially unchanged in mean diameter (19 μm) from the throat (Table 6) to the exit

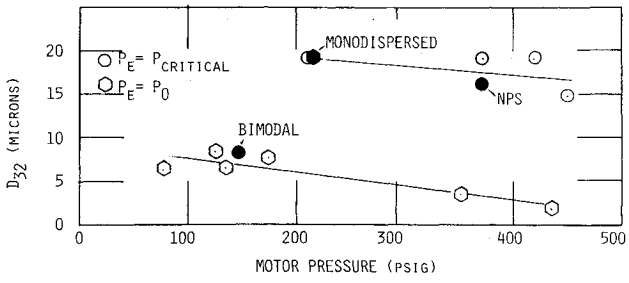

Fig. 8 Nozzle exhaust D_{32} as a function of pressure.

plane (Table 7). The measurements made further aft had one mode centered at the same 19 μm diam. In this location, there were fewer 19-μm particles, and significant numbers of smaller particles were observed in bimodal, trimodal or quadmodal distributions. Thus, particle breakup may have occurred within the exhaust plume. However, additional data are needed to clarify this behavior.

Comparison of the Measurement Techniques

Figure 9 compares the measurements made at the nozzle entrance using the Malvern and NPS systems. The NPS system resulted in significantly smaller values of D_{32} at low pressures. There were two reasons for this behavior. First, the larger particles of the bimodal distributions (40–70 μm) scattered most of their light at smaller angles than could be measured by the NPS system. This was the dominant effect. If the Malvern data (which included small scattering angles) for scattering angles outside the field of view of the NPS system were suppressed, good agreement with the NPS data were obtained. Second, the data-reduction algorithm used for the NPS apparatus assumed a monomodal, upper-limit distribution. At the lower pressures, the Malvern data (operated in the model-independent mode) showed the distributions were bimodal. The effect on D_{32} of assuming a monomodal distribution when it is actually multimodal depends upon the separation between the modes. For example, if Rosin-Rammler or log-normal distributions were assumed, the Malvern would calculate D_{32} values of 19 and 20 μm, respectively, for the trimodal distribution shown in Fig. 3. The actual value for D_{32} (model-independent mode) was 15 μm. In this case, the monomodal distributions were biased towards that portion of the distribution which contained the higher volume fraction. When the multimodal distributions are closely spaced, the monomodal assumption has a much smaller effect on weighted parameters such as D_{32}.

When the pressures were higher, the distributions became monomodal and the particles were within the measurement range of the NPS apparatus. Under these conditions, the results were in much better agreement (Fig. 9).

Table 7 Exhaust scattering measurements using the Malvern ($P_e = P_{ambient}$)

Pressure, psig	Location behind nozzle exit, in.	D_{32}, μm	Type of distribution	Peaks of dominant modes, μm
79	1.7	6.2[a]	Trimodal	2, 6, 15
125	2.7	8.3	Trimodal	2 (weak), 8, 19
135	2.7	6.5	Broad bimodal	4, 19
175	2.7	7.6	Trimodal	2.8, 7, 19
215	0.6	19	Narrow monomodal	19
352	2.7	3.4	Quadmodal	<2, 5.5, 11, 19
436	2.7	1.9	Quadmodal	<2, 4.5, 7, 19

[a]Graphite nozzle with no converging section. Knife-edged orifice with 45 deg half-angle divergence.

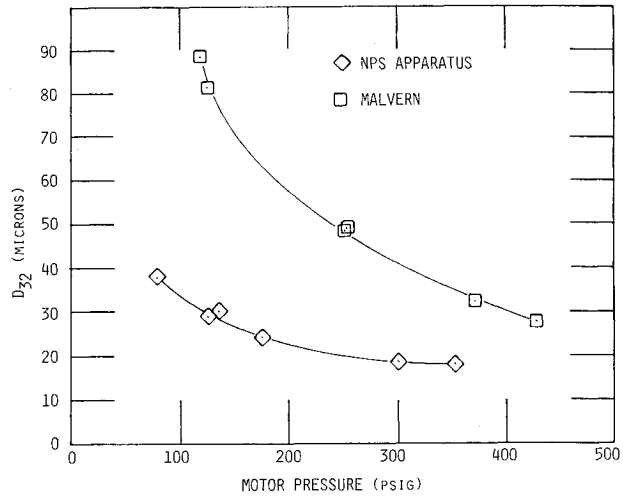

Fig. 9 Comparison of NPS apparatus and Malvern data at Nozzle entrance.

Conclusions and Recommendations

The results of this investigation have demonstrated that laser diffraction methods can used for determining particle sizes in solid-propellant rocket motors. Measurements were successfully made in both the motor chamber and exhaust environments.

The Malvern and the NPS diffraction systems produced data which correlated quite well when the particle distributions were monomodal, and the dominant scattered light was within the field of view of the NPS linear diode array. When the distributions were multimodal and widely spaced, the NPS system did not accurately measure the Sauter mean diameter. This problem resulted from a limited field of view and the data-reduction algorithm. The latter was based upon monomodal distributions. The system could be significantly improved by using larger arrays and by using data-reduction techniques which are based on quadrature methods.[17] The NPS system will always be limited to higher-number density flows since the linear array only intercepts a very small fraction of the light scattered at a given angle.

The motor data suggested that much of the ZrC reacts to form ZrO_2 on or near the propellant surface. Surface agglomeration occurred and the agglomerates were observed to decrease in mean (D_{32}) size as chamber pressure increased. The distributions were trimodal or quadmodal near the surface and shifted more to the smaller sizes as the pressure was increased. In the present motor, the larger particles (probably ZrO_2 or particles with a ZrO_2 surface layer) remained practically unchanged as they passed down the length of the motor port, while the smaller particles (probably ZrC which was ejected from the propellant surface without agglomeration) were consumed.

At low pressure, bimodal particle distributions were observed at the nozzle entrance. At higher pressures (greater than 350 psi) the distributions were monomodal. Particulates broke up in the nozzle converging section to a monomodal distribution with a D_{32} between 15 and 19 μm, independent of the particle size entering the nozzle. Further particle breakup occurred either within the exhaust cone or plume. In the plume the particle distributions were multimodal, with the largest mode centered at the throat particle size of 19 μm and the smallest mode centered at less than 2 μm. As exit Mach number (and inlet pressure) increased, D_{32} decreased.

Acknowledgment

This research was supported by the Air Force Astronautics Laboratory, Edwards AFB, California, by Contract F04611-87-K-0040.

References

[1]Netzer D. W., and Powers, J. P., "Smokeless Propellants," AGARD CP-391, Sept. 1985.

[2]Coats, D. E., Levine, J. N., Nickerson, G. R., Tyson, T. J., Cohen, N. S., Harry, III, D. P., and Price, C. F., "A Computer Program for the Prediction of Solid-Propellant Rocket Motor Performance," Air Force Rocket Propulsion Lab., AFRPL-TR-75-36, Vol. I, July 1975.

[3]Hermsen, R. W., "Aluminum Oxide Particle Size for Solid Rocket Motor Performance Prediction," AIAA Paper 81-0035, Jan. 1981.

[4]Swithenbank, J., Beer, J. M., Taylor, D. S., Abot, D., and McCreath, G. C., "A Laser Diagnostic Technique for the Measurement of Droplet and Particle Size Distribution," *Experimental Diagnostics in Gas Phase Combustion Systems,* Vol. 53, Progress in Astronautics and Aeronautics, AIAA, New York, 1977, pp. 421-447.

[5]Hirleman, E. D., "Nonintrusive Laser-Based Particle Diagnostics," *Combustion Diagnostics by Nonintrusive Methods,* Vol. 92, Progress in Astronautics and Aeronautics, AIAA, New York, 1983, pp. 177-207.

[6]Kerker, M., *The Scattering of Light and Other Electromagnetic Radiation,* Academic, 1969, Chap. 3.

[7]Van de Hulst, H. C., *Light Scattering by Small Particles,* Wiley, New York, 1957.

[8]Powell, E. A., Cassanova, R. A., Bankston, C. P., and Zinn, B., "Combustion-Generated Smoke Diagnostics by Means of Optical Measurement Techniques," AIAA Paper 76-67, Jan. 1976.

[9]Jones, A. R., "Error Contour Charts Relevant to Particle Sizing by Forward Scattered Lobe Measurements," Letter to the Editor, *Journal of Physics, Applied Physics,* No. 13, Sept. 1977, pp. L163-L165.

[10]Hodkinson, J. R., "Particle Sizing by Means of the Forward Scattering Lobe, *Applied Optics,* Vol. 5, No. 5, 1966, pp. 839-844.

[11]Boron, S., and Waldie, B., "Particle Sizing by Forward Lobe Scattered Intensity Ratio Technique: Errors Introduced by Applying Diffraction Theory in the Mie Regime," *Applied Optics,* Vol. 17, No. 10, May 1978, pp. 1644-1648.

[12]Dobbins, R. A., Crocco, L., and Glassman, I., "Measurement of Mean Particle Sizes of Sprays from Diffractively Scattered Light," *AIAA Journal,* Vol. 1, No. 8, Aug. 1963, pp. 1882-1886.

[13]Mugele, R. A., and Evan, H. D., "Droplet Size Distribution in Sprays," *Industrial and Engineering Chemistry,* Vol. 43, No. 6, 1951, pp. 1317-1324.

[14]Buchele, D. R., "Particle Sizing by Measurement of Forward Scattered Light at Two Angles," NASA TP-2156, May 1983.

[15]Harris, R. K., "An Apparatus for Sizing Particulate Matter in Solid Rocket Motors, M.S. Thesis, Naval Postgraduate School, Monterey, CA, June 1984.

[16]Dodge, L. G., Rhodes, D. J., and Reitz, R. D., "Drop Size Measurement Techniques for Sprays: Comparison of MALVERN Laser-Diffraction and Aerometrics Phase/Doppler," *Applied Optics,* Vol. 26, No. 11, June 1987, pp 2144-2154.

[17]Koo, J. M., and Hirleman, E. D., "Comparative Study of Laser Diffraction Analysis Using Integral-Transform Techniques: Factors Affecting the Reconstruction of Droplet Size Distributions," The Combustion Institute, Pittsburgh, PA, Paper 86-18, April, 1986.

[18]Edwards, T. D., Harris, R. K., et. al, "Measurements of Particulates in Solid Propellant Rocket Motors," Air Force Astronautics Lab., Edwards AFB, CA, AFAL TR-87-029, Oct. 1987.

[19]Gulder, O. L., "Multiple Scattering Effects in Drop Sizing of Dense Fuel Sprays by Laser Diffraction," AGARD 70th Symposium of the Propulsion and Energetics Panel on Combustion and Fuels in Gas Turbines, Oct. 1987.

[20]Rudy, T. P., Private communication, Dec. 1987.

[21]Price, E. W., "Combustion of Metallized Propellants," *Fundamentals of Solid-Propellant Combustion,* Vol. 90, edited by M. Summerfield, and K. K. Kuo, Progress in Astronautics and Aeronautics, AIAA, New York, 1984, pp. 479-513.

[22]Lynch, C. T., *CRC Handbook of Material Science,* CRC Press, Cleveland, Ohio, 1975.

[23]Shwartkopk, P., and Kiefer, R., *Refractory Hard Metals Borides, Carbides, Nitrides, and Silicides,* MacMillan, New York, 1953.

[24]Caveny, L. H., and Gany, A., "Breakup of Al/Al_2O_3 Agglomerates in Accelerating Flowfields," AIAA Paper 79-0300, Jan. 1979.